TRENDS IN SCIENCES 2026; 23(3): 11651
https://doi.org/10.48048/tis.2026.11651
RESEARCH ARTICLE

Impact of YSZ Solid Electrolyte on the Efficiency and Photoresponse of Dye-Sensitized Solar Cells

Erma Surya Yuliana[1], Ulfiya Rifqi Azizil Mukaromah[1], Anissa Chairani Alvin Nadhira[1], Poppy Puspitasari[2], Markus Diantoro[1], Muhammad Safwan Abd Aziz[3] and Nandang Mufti[1,4,*]

[1]Department of Physics, Faculty of Mathematics and Natural Sciences, Universitas Negeri Malang, Malang 65145, Indonesia
[2]Department of Mechanical Engineering, Faculty of Engineering, Universitas Negeri Malang, Malang 65145, Indonesia
[3]Laser Center, Ibnu Sina Institute for Scientific and Industrial Research, Universiti Teknologi Malaysia, Johor Bahru 81310, Malaysia
[4]Center of Advanced Materials for Renewable Energy, Universitas Negeri Malang, Malang 65145, Indonesia

([*]Corresponding author's e-mail: nandang.mufti.fmipa@um.ac.id)

Received: 21 August 2025, Revised: 9 September 2025, Accepted: 16 September 2025, Published: 30 November 2025

Abstract

Dye-sensitized solar cells (DSSCs) are an alternative method for converting solar energy into electrical energy and have attracted significant interest due to their environmentally friendly production process, relatively low fabrication cost, and competitive efficiency. This study aims to investigate the efficiency and photoresponse of DSSCs using yttria-stabilized zirconia (YSZ) as a solid electrolyte to replace the conventional liquid electrolyte. The DSSC consists of 4 main components: A photoanode made from mesoporous TiO_2, a counter electrode using carbon/graphene, the dye N719, and YSZ solid electrolyte. Mesoporous TiO_2, YSZ, and graphene were deposited using screen printing, doctor blade, and knife coating methods, while the dye N719 was injected into the film. The samples were characterized using XRD, SEM, and UV-Vis spectroscopy. Based on the analysis result, with the increase of the thickness from 5 - 25 µm, the crystal size was increased from 6.37 - 6.92 nm and porosity was decreased from 63.5% - 58.0%, while the band gap increased (3.34 - 3.37 eV), respectively. The solar cell efficiency and photoresponse were measured using a solar simulator. The highest efficiency achieved was 3.88% for the YSZ thickness. Additionally, the TiO_2/YSZ film demonstrated a rapid response to light exposure, making it a promising material for light sensors.

Keywords: DSSC, Dye N719, TiO_2 mesoporous, Solid electrolyte, Yttria-stabilized zirconia

Introduction

Electrical energy is one of the primary needs nowadays. Energy has a very important role in meeting all the needs of life in the world [1]. People will be encouraged to search for alternative energy as energy needs increase. One alternative energy solution that can be utilized is solar energy, which is abundant and friendly to the environment. Solar energy can be utilized as a power plant with the photovoltaic principle [2]. One of the most developed photovoltaic devices is dye-sensitized solar cells (DSSC). In DSSC, solar energy is converted into electrical energy by transferring electrons from DSSC components [3,4]. These components include photoanodes, counter electrodes, dyes, and electrolytes [5]. Besides that, efficiency plays a vital role in measuring the performance of a solar cell device. To increase efficiency, special treatment for semiconductors is necessary. The treatment may

influence how the dye adheres to the semiconductor layer [6].

Currently, mesoporous TiO_2 is widely developed due to the potential to increase the efficiency of solar cells [7]. Mesoporous TiO_2 has a high band gap (3.4 eV) when compared to ordinary TiO_2 and ZnO [8,9], due to its high specific surface area (112 m^2/g) [10,11], the uniform pore diameter [12], and its potential role in increasing light absorbance [13]. Mesoporous TiO_2 has a high band gap value (3.4 eV) [13], in which light adsorption occurs at the time of dye absorption [8]. Additionally, the presence of pores on the surface of the thin layer maximizes the absorption of the dye [14]. The more dye is absorbed, the more effectively the dye can work. In addition, the thickness of the TiO_2 substantially affects the V_{OC} and J_{SC} since electron transfer, diffusion, and production of current are connected to the thickness of the TiO_2 photoelectrode. Sharma *et al.* [15] showed that the TiO_2 showed the highest efficiency at a 12 µm thickness layer.

The counter electrode used in this study is graphene, which has layers of carbon atoms [16]. Graphene has electrolytic properties as well as high magnetic properties [17]. This material looks promising for use in the present study. This is due to its easy availability [18], high specific surface area (305 m^2/g) [19], and high electrical conductivity (2×10^{-3} S/cm) [20]. Several studies have been conducted, with the majority utilizing liquid electrolytes based on I/I_3^-, demonstrating high-efficiency performance. However, using liquid electrolytes has disadvantages, such as susceptibility to solvent evaporation, leakage, and degradation of electrolyte materials, which can lead to photoanode corrosion [21]. As a solution, the development of solid-state electrolytes for DSSCs presents a promising alternative. Therefore, this study switched to using solid electrolytes. Solid-state electrolytes offer advantages such as improved stability and greater potential for long-term applications. The solid electrolyte that will be applied in this research is an electrolyte based on yttria-stabilized zirconia (YSZ), where this material has high mechanical properties and ionic conductivity (> 1×10^{-3} S/cm) [22,23]. Ionic conductivity is electrical conductivity due to the motion of ionic charge and is a critical parameter required for superionic conductors to be successfully applied as solid electrolytes [24]. The ionic conductivity of YSZ material depends on factors like grain size, amount of dopant, method of production, temperature, etc. [25]. YSZ-based solid electrolytes have a lower environmental footprint when compared to conventional liquid electrolytes in DSSCs because they do not use toxic organic solvents. On the other hand, liquid electrolytes produce emissions and are difficult to recycle, thus increasing the potential for environmental pollution. Thus, overall, YSZ-based solid electrolytes are more environmentally friendly in the long term than liquid electrolytes for DSSC applications [21]. Solovyev *et al.* [26] have reported the electrical properties of YSZ solid electrolyte thin films through current and voltage relationships. The measurement results show that the cell that YSZ thin film electrolyte produces a maximum power density of 425 mW/cm^2 at 600 ℃ [26]. The power density measurement uses a liquid electrolyte of 300 mW/cm^2 at 550 - 600 ℃ [27]. Therefore, this study aimed to determine the crystal structure and optical properties and improve performance in DSSC using YSZ solid electrolyte. This research will combine mesoporous TiO_2 films as photoanodes with YSZ thickness variations of 5, 15 and 25 µm, which are expected to improve efficiency performance.

Materials and methods

Blocking layers were synthesized using 0.5 mL titanium (IV) (tri ethanol) isopropoxide (TTIP) mixed with 5 mL isopropanol and then stirred for 2 h at 500 rpm at room temperature. Deposition on ITO glass by the spin method at 3,000 rpm. Then, it was heated on a hot plate at temperatures of 100, 300 and 500 ℃ for 15, 15 and 30 min, respectively. To synthesize TiO_2 mesoporous, 0.25 g of PEG, 1 g of TiO_2, and 1 mL of HNO_3 were mixed and ground for a total of 70 min. The deposition of TiO_2 on ITO glass was done using the screen-printing method. The film was then heated on a hot plate at 100, 300 and 500 ℃ for 15, 15 and 30 min, respectively. Next, post-treatment was carried out on the ITO/TiO_2 film. 100 µL TTIP was added to a 20 mL isopropanol stirrer for 30 min at 500 rpm at room temperature. Then, heat it in the oven for 30 min. Clean the sample with ethanol p.a., then heat it on a hot plate at a temperature of 500 ℃ for 30 min. After that, synthesize the solid electrolyte. YSZ was heated at 1,200 ℃ for 2 h. Two g of YSZ powder were crushed for 30 min, then 300 µL isopropanol and 180 µL HNO_3

p.a were added. Deposition on the substrate using the doctor blade method with varying thicknesses of 5, 15 and 25µm. Heat at 100 ℃ for 1 h. To synthesize the carbon counter electrode, 0.02 g of graphene was mixed with 0.02 g of PVDF and dissolved in 2 mL of NMP. Then, stir at 600 rpm for 24 h. Deposition on a silicon wafer with the knife coating method and keep it in the oven for 1 h at 100 ℃. The N719 dye was injected into the film before the characterization to finish the fabrication. Illustrate the DSSC using YSZ electrolyte, as shown in **Figure 2**.

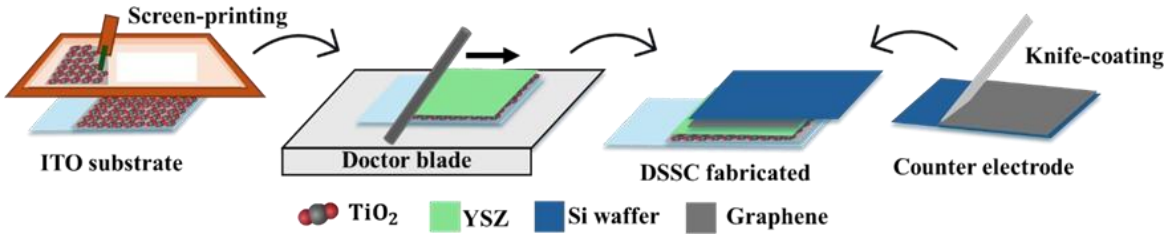

Figure 1 Schematic illustration of the deposition mechanism for TiO_2/YSZ films and graphene film.

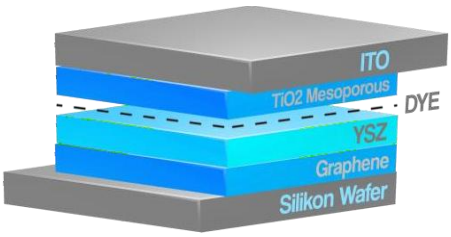

Figure 2 Illustrate of TiO_2/YSZ Film.

The successfully fabricated TiO_2 mesoporous and TiO_2/YSZ films were then characterized by X-ray diffraction (XRD) using a PANalytical X'Pert Pro with a monochromated Cu-Kα source (λ = 1540 Å) to determine the crystal structure. Ultraviolet-visible (UV-Vis) spectroscopy, using an Analytik Jena Specord 200 plus, was performed to determine the band gap and absorbance values of the TiO_2/YSZ film. A scanning electron microscope (SEM) detected the thickness of the layered material. In addition, low-cost solar simulators abet technologies model 10500, providing a constant light intensity of 100 mW/cm², and photodetector measurements were used to determine the efficiency of this TiO_2 mesoporous/YSZ film. The TiO_2/YSZ thin films were labeled as YSZ-5, YSZ-15, and YSZ-25, corresponding to YSZ thicknesses of 5, 15 and 25 µm.

Results and discussion

Figure 3(a) shows the diffraction pattern of TiO_2 mesoporous. Some of the TiO_2 mesoporous peaks formed are at angles of 25.19°, 37.66°, 53.75°, 55°, 70.26°, and 74.97°. All peaks correspond to the mesoporous tetragonal TiO_2 anatase phase with the 41/amd space group, according to a study conducted by Singh *et al.* [28]. Based on the results of the analysis using Rietica Software with code AMCSD 0019093, there are other ITO peaks found at angles of 30.1°, 35.13°, 47.93°, 50.59°, 60.02°, and 62.57°. The lattice parameters of the mesoporous TiO_2 sample from Rietica showed a = b and c of 3.786 and 9.520 Å, respectively, which aligns with previous research by Wang *et al.* [29]. Crystal size is obtained from the calculation of the Scherrer Eq. (1):

$$D = \frac{K\lambda}{\beta \cos\theta} \quad (1)$$

The K value is 0.9, which is the value of the Scherrer constant and depends on the crystal form [30]. λ is the wavelength that represents X-rays with a magnitude of 0.154056 nm. β is the dominant peak's full width at half maximum (FWHM) value shown in **Table 1**. θ is the diffraction peak angle in rad. So, the crystal size obtained at the hkl peak (101) is 7.36 nm. **Figure 2(b)** shows the diffraction pattern of TiO_2/YSZ films with varying YSZ thickness. The thicknesses given are

5, 15, and 25 µm, respectively. Based on the XRD results, the thicker the YSZ, the higher the YSZ peak. The YSZ has a cubic crystal structure with a 3 m Fm space group [31]. Some of the YSZ peaks that are formed are at angles of 30.21°, 31.51°, 35.13°, 59.91°, 62.79°, and 74.29°. According to the analysis, the lattice parameters of YSZ are $a = b = c = 5.154$ Å, which aligns with previous research by Wang *et al.* [32]. Meanwhile, the smaller the mesoporous TiO_2 peak detected. This is because YSZ is more dominant when compared to TiO_2 at the thickest thickness.

The surface morphology, cross-section, and particle size distribution of the films are shown in **Figure 4**. The figure shows the TiO_2 thickness of 10.4 µm and the diameter analysis curve for mesoporous TiO_2 with an average 400 - 500 nm diameter. This is following research conducted by Zhang *et al.* [33], which resulted in a diameter of 200 - 500 nm. The YSZ surface morphology with thickness variations of 5, 15, and 25 µm, respectively. The SEM analysis shows that the different thicknesses of the doctor blade method did not contribute much to surface morphology. On the other hand, agglomeration of the YSZ particles is evident due to the high-temperature treatment. **Table 1** shows the porous diameter and porosity of TiO_2 and TiO_2 mesoporous/YSZ in several variations. It can be seen that the thicker the YSZ, the bigger the porous diameter appears. This corresponds to the XRD analysis, as explained previously. The agglomeration also resulted in a larger particle size of YSZ [34]. It can be seen from the graph that the thicker the YSZ, the lower the porosity value would be. The porosity values for each variation of YSZ thickness are provided in **Table 1**. These values can be calculated using Eq. (2) [35].

$$Porosity\ (\%) = \left(\frac{Volume\ of\ Voids}{Total\ Volume}\right) \times 100\% \quad (2)$$

This relates to the results of the particle size obtained, which shows that the lower the average diameter value obtained, the higher the porosity value. If the porosity value is greater, the dye absorption will also be maximized because the active surface area produced is greater [36]. A larger active surface area can improve overall solar cell performance [37]. This is due to the larger active surface area. The cross-section results from the SEM with the variation of YSZ are 5, 15 and 25 µm, respectively. The results are pretty good. Several things influence the thickness of this film. The thickness of the TiO_2 mesoporous layer is affected during the screen-printing process, so the thickness is not controlled for each sample. Meanwhile, the thickness of the YSZ solid electrolyte is adjusted during the doctor blade process.

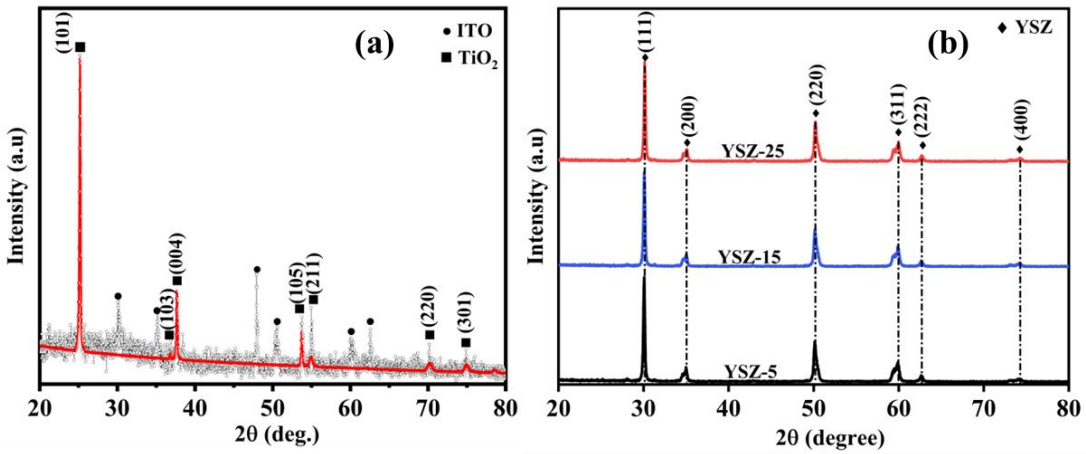

Figure 3 Diffraction pattern of (a) TiO_2 mesoporous, (b) TiO_2/YSZ films.

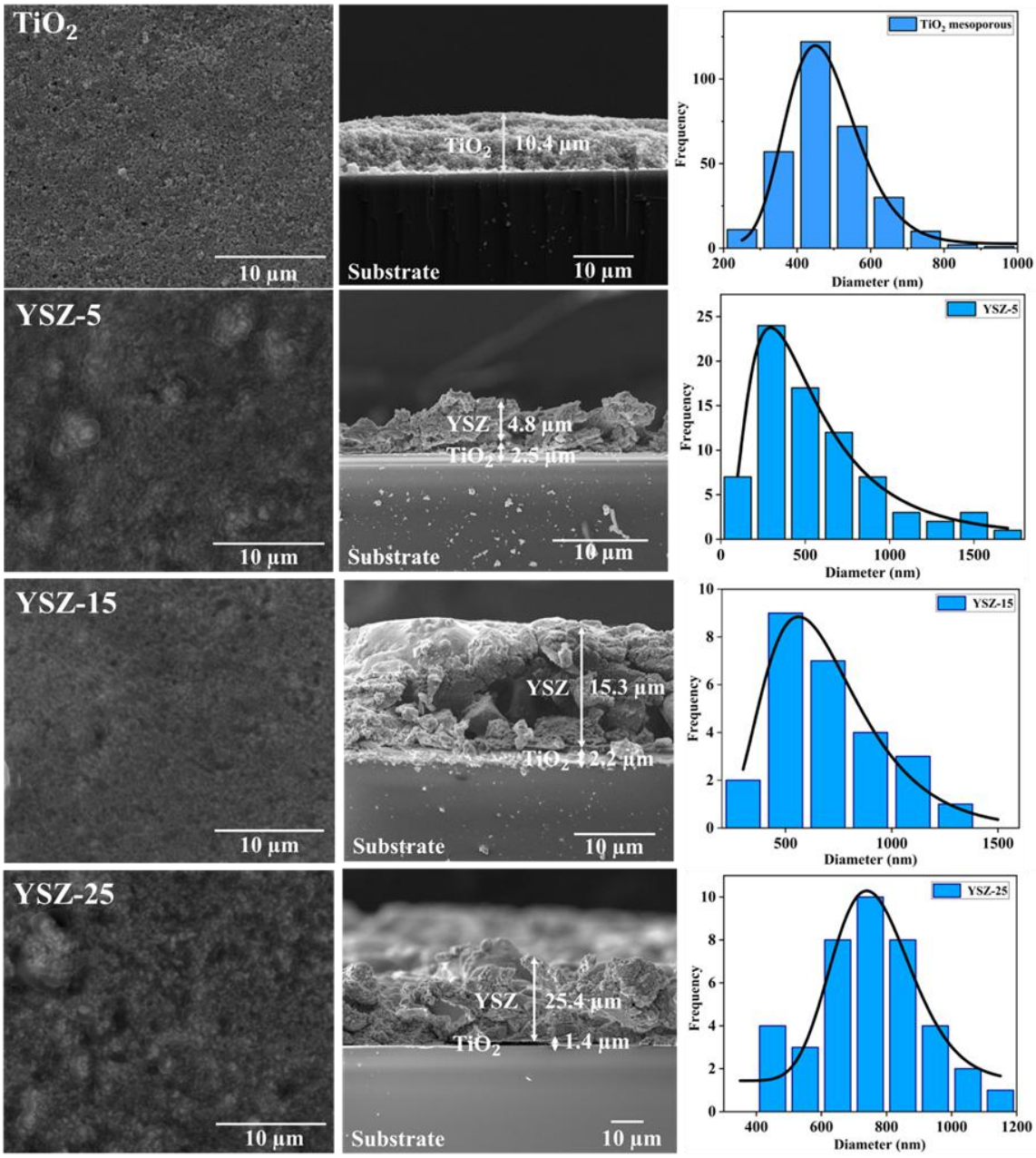

Figure 4 Morphology, cross-section, and particle size distribution of TiO_2 and TiO_2/YSZ with a magnitude of 10,000×.

Table 1 The crystal size, FWHM, porous diameter, porosity of TiO_2 mesoporous, and several thickness variations of YSZ.

Sample	Crystal Size (nm)	FWHM (rad)	Miller index (hkl)	Porous diameter (nm)	Porosity (%)
TiO_2 mesoporous	7.36	0.0024	1 0 1	469.4 ± 0.3	55.9
YSZ-5	6.37	0.0034	1 1 1	474.1 ± 0.3	63.5
YSZ-15	6.63	0.0027	1 1 1	655.3 ± 0.4	60.4
YSZ-25	6.92	0.0031	1 1 1	758.9 ± 0.2	58.0

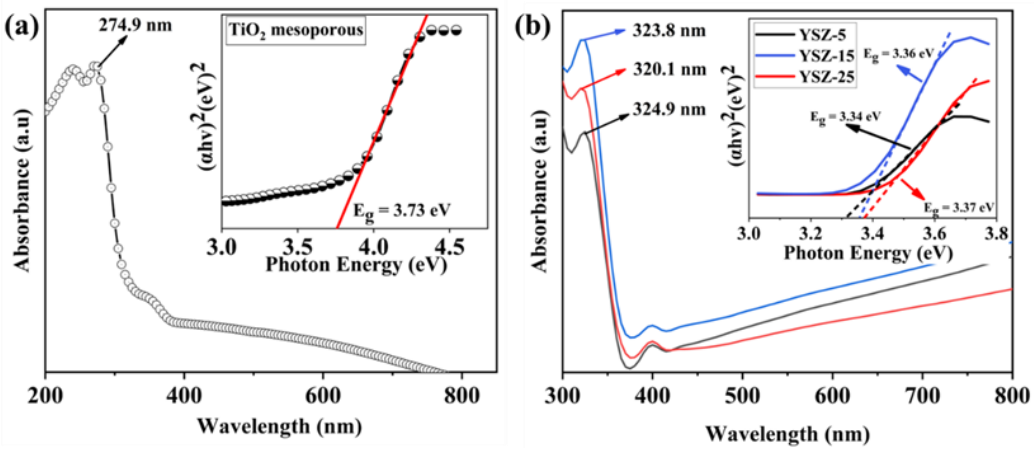

Figure 5 The absorbance and fitting bandgap of (a) TiO_2 mesoporous and (b) TiO_2/YSZ films in different thicknesses.

In **Figure 5**, the results of absorbance data processing of the absorbance of TiO_2/YSZ show a wavelength range of 300 - 800 nm. Currently, TiO_2/YSZ films are known only to be able to absorb light at this wavelength due to the band gap. This causes the absorbance value to be relatively high [38]. In the figure, it can also be seen that the absorbance wavelength of this film is around 300 nm. According to research by Sutherland *et al.* [39], this can happen because this film is closer to the ultraviolet wavelength spectrum. Many factors can affect the size of an absorbance value. One of these factors is the tire gap value, grain size, and the amount of oxygen contained in the material [40]. The band gap value of TiO_2 mesoporous and the band gap of TiO_2/YSZ at 5, 15, and 25 µm variations. The TiO_2 mesoporous band gap is 3.73 eV. This value is quite significant compared to the absorbance value of ordinary TiO_2, whose band gap is around 3.2 eV [41]. This is the same as Maddu's study due to the presence of other materials, such as PEG material, which can result in high band gap values [42]. And the thicker the thickness of TiO_2 mesoporous/YSZ, the greater the band gap value would be.

Table 2 Absorbance and band gap of TiO_2 mesoporous and TiO_2/YSZ films.

Sample	Absorbance (nm)	Band gap (eV)
TiO_2 mesoporous	274.9	3.73
YSZ-5	324.9	3.34
YSZ-15	320.1	3.36
YSZ-25	323.8	3.37

Table 2 presents the absorbance and band gap of TiO_2 mesoporous/YSZ at varying thicknesses. The results show that the highest absorbance value occurs in the band with the smallest band gap. Even though it does not look much different when viewed from the crystal size, the thinnest YSZ layer is obtained, which has the smallest particle size, so the surface area obtained in the thin layer is the largest. In addition, the smaller the band gap, the easier it is to transfer electrons from the valence band to the conduction band [43]. The photodetector test has a function to determine how quickly the light responds to the sample. In this study, testing was carried out by irradiating the sample with light for 10 s and not being exposed to light for 10 s so that it can be seen how fast the response of the sample.

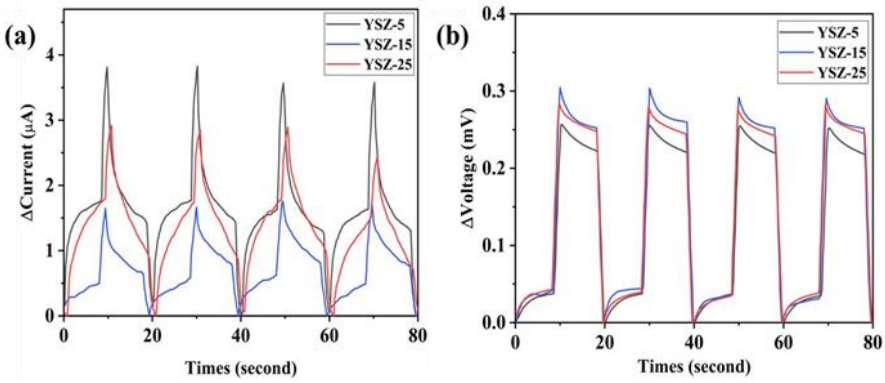

Figure 6 Photoresponse of TiO_2 mesoporous/YSZ.

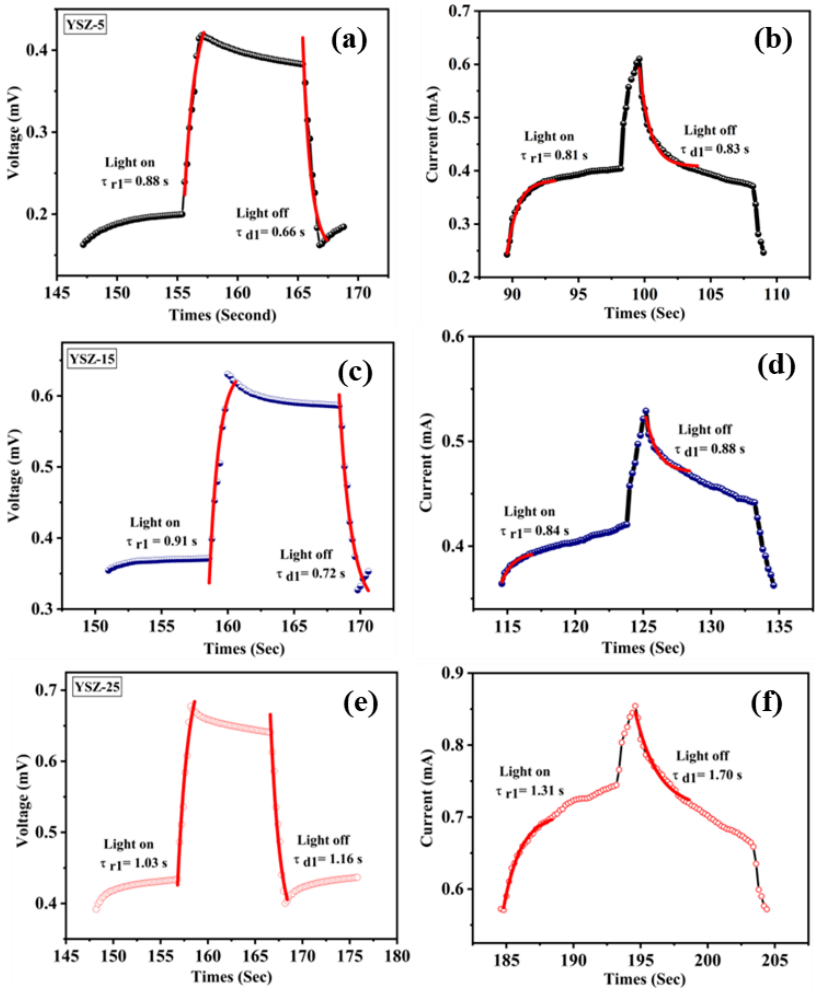

Figure 7 Fitting Photoresponse of Voltage and Current of TiO_2/YSZ film in different thicknesses (a), (b) 5 μm, (c), (d) 15 μm, and (e), (f) 25 μm.

Figure 6(a) is a photoresponse graph of TiO_2/YSZ currents. In contrast, **Figure 9(b)** is a photoresponse graph for measuring TiO_2/YSZ voltages, testing this sample using a solar simulator with a laser power of 100 mW/cm^2. The graph shows that the TiO_2 mesoporous/YSZ sample responds well. When the sample is given solar simulator light, the photocurrent can show a rapid increase, and when the sample is not given light, the sample responds well without reaching saturation [44].

Figure 7 presents the voltage and current photoresponse fitting of TiO_2/YSZ films at different

thicknesses. Under light exposure (Light on), the thinnest film shows the most effective response. In darkness (Light off), a thinner TiO_2/YSZ film also responds more rapidly, with response times under 1 s. This high responsiveness to light changes makes the TiO_2/YSZ film well-suited for applications requiring fast detection or reaction to light exposure, such as in sensors, aligning with the efficiency results obtained.

The current photoresponse fitting similarly shows that, under illuminated conditions (Light on), the thinnest sample achieves the best results, and the same trend is observed in darkness (Light off) as well. Thinner TiO_2/YSZ films produce faster responses, with response times consistently within 1 s, indicating strong performance. The sharp peak observed in the current is due to synchronization when switching from light to dark or vice versa [45]. **Table 3** provides a summary of the photoresponse fittings for TiO_2/YSZ films at various thicknesses.

Table 3 Voltage and current photoresponse fitting of TiO_2/YSZ films.

Sample	Voltage		Current	
	Light on (τ_{r1}) (s)	Light Off (τ_{d1}) (s)	Light on (τ_{r1}) (s)	Light Off (τ_{d1}) (s)
YSZ-5	0.81	0.66	0.81	0.83
YSZ-15	0.91	0.72	0.84	0.88
YSZ-25	1.03	1.16	1.31	1.70

The performance of DSSC based on solid electrolyte YSZ that has been successfully fabricated is then tested I-V with a solar simulator.

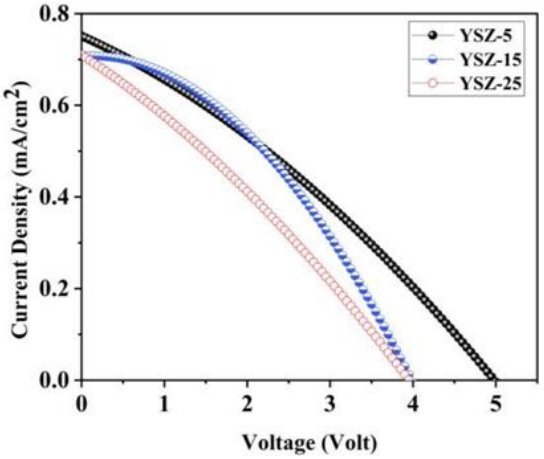

Figure 8 Efficiency of TiO_2/YSZ films in different thicknesses.

Figure 8 shows the efficiency fittings of TiO_2 mesoporous/YSZ in different thicknesses, 5, 15, and 25 µm. It can be concluded that the thinner the thickness of mesoporous TiO_2 mesoporous/YSZ, the greater the efficiency value. This is following research conducted by Takayanagi *et al.* [46]. So, the thinner the film thickness, the better the conductivity. The oxygen ion conductivity arises due to YSZ oxygen vacancies [43]. Increasing the conductivity for thin films can change the structure around the vacancies on the surface of YSZ grains [46,47]. The following is a table of the results of fitting TiO_2 mesoporous/YSZ in several thicknesses shown in **Table 4**.

Table 4 Efficiency parameters TiO_2 mesoporous/YSZ.

Parameters	YSZ-5	YSZ-15	YSZ-25
Rs (Ω)	17.10	6.63	4.12
Isc (mA)	0.08	0.08	0.07
Jsc (mA/cm^2)	0.78	0.76	0.72
Voc (V)	4.76	4.76	4.10
Fill Factor	0.42	0.41	0.35
Pmax (W)	0.16	0.15	0.10
Imax (mA)	0.06	0.07	0.03
Vmax (V)	2.65	2.10	2.95
Efficiency (%)	3.88	3.71	2.76

Based on the results obtained, it can be concluded that the thicker the YSZ, the lower the efficiency. This can happen because the conductivity of YSZ thick films is lower [48]. In addition, YSZ-5 has a smaller crystal size, so dye absorption is maximized due to the greater active surface area produced [49].

Conclusions

DSSC based YSZ solid electrolyte prepared using doctorblade method, with the thickness varying from 5 to 25 μm. Based on data analysis, increasing the YSZ thickness resulted in a increase in crystal size (6.37 - 6.92 nm) and band gap (3.34 - 3.37 eV), while the porosity slightly decreased (63.5% - 58.0%). It can be concluded that the thicker YSZ has the smallest crystal size correspond to leading to a higher porosity due to its larger active surface area. The current and voltage fitting results indicated that as the film thickness decreases, the response to light becomes faster exhibited superior photoelectric response. Finally, the highest efficiency of 3.88% was achieved at the lowest YSZ thickness, likely due to the reduced conductivity in thicker YSZ films. Consequently, reducing the YSZ thickness appears to enhance the efficiency of solar cell devices. Additionally, the TiO_2/YSZ film exhibits a quick response to light exposure, making it a promising material for solar cell.

Acknowledgements

This research was funded by Universitas Negeri Malang, Indonesia through the Matching Grant program in collaboration with the Universiti Teknologi Malaysia, Malaysia under grant number 4.4.634/UN32.14.1/LT/2024.

Declaration of Generative AI in Scientific Writing

Only minimal assistance was used from Grammarly for paraphrasing selected sentences. All scientific content, interpretation, and conclusions were developed independently by the author.

CRediT Author Statement

Erma Surya Yuliana: Methodology, Visualization, and Writing –original draft. **Ulfiya Rifqi Azizil Mukaromah:** Data curation, Formal analysis, and Investigation. **Anissa Chairani Alvin Nadhira:** Data curation and Formal analysis. **Poppy Puspitasari:** Validation and Supervision. **Markus Diantoro:** Validation and Methodology. **Muhammad Safwan Abd Aziz:** Supervision and Methodology. **Nandang Mufti:** Supervision, Validation, and Writing-review and editing.

References

[1] MJB Kabeyi and OA Olanrewaju. Sustainable energy transition for renewable and low carbon grid electricity generation and supply. *Frontiers in Energy Research* 2022; **9**, 743114.

[2] A Rahman, O Farrok and MM Haque. Environmental impact of renewable energy source based electrical power plants: Solar, wind, hydroelectric, biomass, geothermal, tidal, ocean, and osmotic. *Renewable and Sustainable Energy Reviews* 2022; **161**, 112279.

[3] R Sasikumar, S Thirumalaisamy, B Kim and B Hwang. Dye-sensitized solar cells: Insights and research divergence towards alternatives. *Renewable and Sustainable Energy Reviews* 2024; **199**, 114549.

[4] NH Rased, B Vengadaesvaran, SRS Raihan and NA Rahim. *Introduction to solar energy and its conversion into electrical energy by using dye-sensitized solar cells. In*: SJ Dhoble, NT Kalyani, B Vengadaesvaran and AK Arof (Eds.). Energy materials. Elsevier, Amsterdam, Netherlands, 2021, p. 139-178.

[5] G Richhariya, A Kumar, AK Shukla, KN Shukla and BC Meikap. Effect of different counter electrodes on power conversion efficiency of DSSCs. *Journal of Electronic Materials* 2023; **52(1)**, 60-71.

[6] H Zhou, M Aftabuzzaman, Masud, SH Kang and HK Kim. Key materials and fabrication strategies for high-performance dye-sensitized solar cells: Comprehensive comparison and perspective. *ACS Energy Letters* 2025; **10(2)**, 881-895.

[7] CY Hsu, HNK Al-Salman, ZH Mahmoud, RM Ahmed and AF Dawood. Improvement of the photoelectric dye sensitized solar cell performance using Fe/S-TiO_2 nanoparticles as photoanode electrode. *Scientific Reports* 2024; **14(1)**, 4931.

[8] V Paranthaman, KS Devi, KB Bhojanaa, V Aravindan, G Raman, RS Kumar, C Doroody, RK Rajamony and PS Krishnan. Experimental and theoretical insights into enhanced light harvesting in dye-sensitized solar cells via Au@ TiO_2 core-shell and $BaTiO_3$ nanoparticles. *Journal of the Taiwan Institute of Chemical Engineers* 2024; **165**, 105778.

[9] V Leela Devi, D De, P Kuchhal and RK Pachauri. Photovoltaic performance of TiO_2 and ZnO nanostructures in anthocyanin dye-sensitized solar cells. *Clean Energy* 2024; **8(5)**, 144-156.

[10] Y Yan, Y Zhang, Y Zhao, F Ding, Y Lei, Y Wang, J Zhou and W Kang. Review on TiO_2 nanostructured photoanode and novel dyes for dye-sensitized solar cells application. *Journal of Materials Science* 2025; **60**, 4975-5005.

[11] Y Zhang, H Tao, H Wang, J Hao, Y Liu and Y Yuan. Sol-gel synthesis of magnesium doped TiO_2 thin film and its application in dye sensitized solar cell. *Optical Materials* 2025; **158**, 116446.

[12] CP Pasigon. Performance of dye-sensitized solar cell with carrot-based dyes in deep eutectic solvent and KI/I_2 electrolytes. *Trends in Sciences* 2025; **22(7)**, 10041.

[13] BK Korir, JK Kibet and SM Ngari. A review on the current status of dye-sensitized solar cells: Toward sustainable energy. *Energy Science & Engineering* 2024; **12(8)**, 3188-3226.

[14] AI Rafieh, P Ekanayake, H Nakajima, AH Mahadi, M Abu, MF Don and CM Lim. Enhanced N719 dye adsorption onto Ca and La doped mesoporous TiO_2 anodes for Dye-sensitized solar cells. *Journal of Electronic Materials* 2021; **50(10)**, 5788-5795.

[15] SJ Sharma, J Prasad, SS Soni and N Sekar. The impact of anchoring groups on the efficiency of dye-sensitized solar cells: 2-cyanoacrylic acid vs. ethyl 2-cyanoacrylate. *Journal of Photochemistry and Photobiology A: Chemistry* 2023; **444**, 114915.

[16] T Xia, J Cao, MA Bissett, H Waring, Y Xiang, G Pinter, AV Kretinin, P Yang, Y Zhu, X Zhao, SA Hodge, T Thomson and IA Kinloch. Graphenization of graphene oxide films for strongly anisotropic thermal conduction and high electromagnetic interference shielding. *Carbon* 2023; **215**, 118496.

[17] VAF Samson, SB Bernadsha, JF Britto, MVA Raj and J Madhavan. Synthesis of rGO/$NiFe_2O_4$ nanocomposite as an alternative counter electrode material to fabricate Pt-free efficient dye sensitized solar cells. *Diamond and Related Materials* 2022; **130**, 109406.

[18] SN Tamilselvan and S Shanmugan. Towards sustainable solar cells: Unveiling the latest developments in bio-nano materials for enhanced DSSC efficiency. *Clean Energy* 2024; **8(3)**, 238-257.

[19] ZY Yang, LJ Jin, GQ Lu, QQ Xiao, YX Zhang, L Jing, XX Zhang, YM Yan and KN Sun. Sponge-templated preparation of high surface area graphene with ultrahigh capacitive deionization performance. *Advanced Functional Materials* 2014; **24(25)**, 3917-3925.

[20] M Kashif, E Jafaar, SK Sahari, FW Low, ND Hoa, A Ahmad, A Abbas, Z Ngaini, M Shafa and A Qurashi. Organic sensitization of graphene oxide and reduced graphene oxide thin films for photovoltaic applications. *International Journal of Energy Research* 2021; **45(6)**, 9657-9666.

[21] Y Zhang, B Liu, L Xu, Z Ding, R Yang and S Wang. Failure mechanism analysis and emerging strategies for enhancing the photoelectrochemical stability of photoanodes. *ChemSusChem* 2025; **18(2)**, e202401420.

[22] DJ Brett, A Atkinson, NP Brandon and SJ Skinner. Intermediate temperature solid oxide fuel cells. *Chemical Society Reviews* 2008; **37(8)**, 1568-1578.

[23] SPS Badwal. Zirconia-based solid electrolytes: Microstructure, stability and ionic conductivity. *Solid State Ionics* 1992; **52(1-3)**, 23-32.

[24] Y Wang, Y Wu, Z Wang, L Chen, H Li and F Wu. Doping strategy and mechanism for oxide and sulfide solid electrolytes with high ionic conductivity. *Journal of Materials Chemistry A* 2022; **10(9)**, 4517-4532.

[25] I Danilenko, O Gorban, A Shylo, L Akhkozov, S Gorban, G Lasko and V Mysovets. Determination of the nature of the co-doping effect on the structure, mechanical properties and ionic conductivity of SOFC electrolyte based on YSZ. *Solid State Ionics* 2024; **412**, 116581.

[26] AA Solovyev, NS Sochugov, SV Rabotkin, AV Shipilova, IV Ionov, AN Kovalchuk and AO Borduleva. Application of PVD methods to solid oxide fuel cells. *Applied Surface Science* 2014; **310**, 272-277.

[27] R Raza, Z Gao, T Singh, G Singh, S Li and B Zhu. $LiAlO_2$-$LiNaCO_3$ composite electrolyte for solid oxide fuel cells. *Journal of Nanoscience and Nanotechnology* 2011; **11(6)**, 5402-5407.

[28] I Sta, M Jlassi, M Hajji, MF Boujmil, R Jerbi, M Kandyla, M Kompitsas and H Ezzaouia. Structural and optical properties of TiO_2 thin films prepared by spin coating. *Journal of Sol-Gel Science and Technology* 2014; **72**, 421-427.

[29] C Wang, L Yin, L Zhang, Y Qi, N Lun and N Liu. Large scale synthesis and gas-sensing properties of anatase TiO_2 3-dimensional hierarchical nanostructures. *Langmuir* 2010; **26(15)**, 12841-12848.

[30] N Mufti, IK Laila, R Idiawati, A Fuad, A Hidayat and A Taufiq. The effect of growth temperature on the characteristics of ZnO Nanorods and its optical properties. *Journal of Physics: Conference Series* 2018; **1057(1)**, 012005.

[31] N Ishizawa, Y Matsushima, M Hayashi and M Ueki. Synchrotron radiation study of yttria-stabilized zirconia, $Zr_{0.758}Y_{0.242}$ $O_{1.879}$. *Acta Crystallographica Section B, Structural Science* 1999; **55(5)**, 726-735.

[32] H Wang, RB Dinwiddie and WD Porter. Development of a thermal transport database for air plasma sprayed ZrO_2-Y_2O_3 thermal barrier coatings. *Journal of Thermal Spray Technology* 2010; **19**, 879-883.

[33] Y Zhang, G Li, Y Wu, Y Luo and L Zhang. The formation of mesoporous TiO_2 spheres via a facile chemical process. *The Journal of Physical Chemistry B* 2005; **109(12)**, 5478-5481.

[34] N Mufti, F Ansar, E Latifah, M Dioktyanto, ASP Dewi, MTH Abadi, ET Sari, BH Arrosyid, A Noviyanto and A Arramel. Characterization and performance evaluation of yttria-stabilized zirconia (YSZ) thickness on ZnO nanorods-based photoelectrochemical cell. *Key Engineering Materials* 2023; **950**, 55-62.

[35] M Abdullah and K Khairurrijal. A simple method for determining surface porosity based on SEM images using OriginPro software. *Indonesian Journal of Physics* 2009; **20(2)**, 37-40.

[36] ES Yuliana, ACA Nadhira, N Mufti, M Diantoro and P Puspitasari. A brief study of the carbon counter electrode for photosensor based on DSSC. *E3S Web of Conferences* 2024; **473**, 01005.

[37] ACA Nadhira, N Mufti, MS Aziz, ET Sari, ES Yuliana, MTH Abadi, ASP Dewi, P Puspitasari, M Diantoro and H Setiyanto. The brief study of ZnO/PEDOT: PSS counter electrode in DSSC based on solid electrolyte YSZ. *Materials Science for Energy Technologies* 2024; **7**, 309-317.

[38] X Tan, S Xu, X Wang, F Liu, BA Goodman, D Xiong and W Deng. Preparation and optical properties of samaria-doped yttria-stabilized zirconia single crystals. *Journal of the American Ceramic Society* 2019; **102(11)**, 6863-6871.

[39] JC Sutherland and Griffin. Absorption spectrum of DNA for wavelengths greater than 300 nm. *Radiation Research* 1981; **86(3)**, 399-410.

[40] AS Ahmed, ML Singla, S Tabassum, AH Naqvi and A Azam. Band gap narrowing and fluorescence properties of nickel doped SnO_2 nanoparticles. *Journal of Luminescence* 2011; **131(1)**, 1-6.

[41] DA Hanaor, MH Assadi, S Li, A Yu and CC Sorrell. Ab initio study of phase stability in doped TiO_2. *Computational Mechanics* 2012; **50**, 185-194.

[42] A Maddu, R Purwati and M Kurniat. Effects of poly-ethylene glycol (PEG) template on structural and optical properties of nanocrystalline titanium dioxide (TiO_2) films. *Journal of Ceramic Processing Research* 2016; **17(4)**, 360-364.

[43] W Zhu and H Xiao. First-principles band gap criterion for impact sensitivity of energetic crystals: A review. *Structural Chemistry* 2010; **21**, 657-665.

[44] K Keem, H Kim, GT Kim, JS Lee, B Min, K Cho, MY Sung and S Kim. Photocurrent in ZnO nanowires grown from Au electrodes. *Applied Physics Letters* 2004; **84(22)**, 4376-4378.

[45] Y Zhang, DJ Hellebusch, ND Bronstein, C Ko, DF Ogletree, M Salmeron and AP Alivisatos. Ultrasensitive photodetectors exploiting electrostatic trapping and percolation transport. *Nature Communications* 2016; **7(1)**, 11924.

[46] M Takayanagi, T Tsuchiya, K Kawamura, M Minohara, K Horiba, H Kumigashira and T Higuchi. Thickness-dependent surface proton conduction in (111) oriented yttria-stabilized zirconia thin film. *Solid State Ionics* 2017; **311**, 46-51.

[47] N Mufti, ET Sari, MTH Abadi, ASP Dewi, M Diantoro, MS Aziz, Zulhadjri, H Setiyanto, Sunaryono and P Puspitasari. Effect of activation temperature of Yttria Stabilized Zirconia (YSZ)/ZnO nanorods thin film on photoelectrochemical cell performance. *Journal of Materials Research and Technology* 2022; **20**, 2348-2357.

[48] ME Yeoh, KY Chan, HY Wong, PL Low, GSH Thien, ZN Ng, HCA Murthy and R Balachandran. Hydrothermal duration effect on the self-assembled TiO_2 photo-anode for DSSC application. *Optical Materials* 2023; **141**, 113907.

[49] A Noor, M Hamdini, S Ramadina and Y Tiandho. Dye-sensitized solar cell-based photovoltaic thermal for ethanol distillation: A narrative review. *Jurnal Geliga Sains: Jurnal Pendidikan Fisika* 2020; **8(2)**, 123-131.